Robust Registration of Mouse Brain Slices with Severe Histological Artifacts

Nitin Agarwal*
Dept. Computer Science
Univ. of California, Irvine

Xiangmin Xu
Dept. Anatomy, Neurobiology
Univ. of California, Irvine

M. Gopi
Dept. Computer Science
Univ. of California, Irvine

ABSTRACT

Brain mapping research is facilitated by first aligning digital images of mouse brain slices to standardized atlas framework such as the Allen Reference Atlas (ARA). However, conventional processing of these brain slices introduces many histological artifacts such as tears and missing regions in the tissue, which make the automatic alignment process extremely challenging. We present an end-to-end fully automatic registration pipeline for alignment of digital images of mouse brain slices that may have histological artifacts, to a standardized atlas space. We use a geometric approach where we first align the bounding box of convex hulls of brain slice contours and atlas template contours, which are extracted using a variant of Canny edge detector. We then detect the artifacts using Constrained Delaunay Triangulation (CDT) and remove them from the contours before performing global alignment of points using iterative closest point (ICP). This is followed by a final non-linear registration by solving the Laplace's equation with Dirichlet boundary conditions. We tested our algorithm on 200 mouse brain slice images including slices acquired from conventional processing techniques having major histological artifacts, and from serial two-photon tomography (STPT) with no major artifacts. We show significant improvement over other registration techniques, both qualitatively and quantitatively, in all slices especially on slices with significant histological artifacts.

CCS Concepts

•**Computing methodologies** → **Image processing;** Matching; •**Theory of computation** → *Computational geometry;*

Keywords

Non-Linear Registration; Image Artifacts; Histology; Mouse Brain; Allen Reference Atlas; Point Correspondences

*Email of corresponding author: agarwal@ics.uci.edu

ICVGIP, December 18-22, 2016, Guwahati, India

DOI: http://dx.doi.org/10.1145/3009977.3010053

1. INTRODUCTION

Modern neuroscience is increasingly exploiting three-dimensional digital brain models as a means for understanding complex brain anatomy, localizing experimental data, and planning experiments. Although 3D imaging methods such as MRI and CT scans provide volumetric data, to understand the brain connectomics and how the brain circuit works, much higher resolution imaging methods are required. 2D imaging methods, such as optical microscopy, typically generate serial sections with much higher resolution than MRI or CT scans. Automatic alignment and reconstruction of these 2D sections in 3D therefore becomes important for understanding detail anatomical structures and neuronal connections.

Neuroscience researchers prefer studying mouse brains due to its physiological and genetic similarity to humans, the ease with which its genome can be manipulated, and the ability to train mice to perform behavioural tasks relevant to human cognitive processes. To generate tissue slices for microscope imaging, most neuroanatomist follow an extremely tedious and manual procedure. While the mouse is alive, they first inject its brain with various fluorescent markers targeting specific gene expressions. After which, the mouse is anesthetized and its brain is extracted from the skull. This is followed by slicing the brain tissue into thin serial sections, staining of these sections and mounting them onto the glass slides for high-resolution imaging. There are several advantages of slicing tissues into thin sections, such as focussed images (no depth of focus issue) and accurate 3D reconstruction. However, manual handling and thin tissue sectioning of the brain produces severe deformations making many post processing operations such as automatic alignment and reconstruction extremely challenging. These deformations can be broadly categorized either as *global 3D deformations*, which may happen during extraction of the brain from the skull, physical effects like gravity during mounting, etc. or *slice specific 2D deformations*, which are very common tissue artifacts introduced during sample preparations including serial sectioning of the brain (shearing and tearing) and mounting slices on glass slides (tearing, folding, absence or displacement of small parts from some sections). Though there have been some work on detection and correction of these artifacts (Section 2), most of them are either semi-automatic or use information from neighbouring slices making them not scalable.

Another big challenge of imaging mouse brain is in the interpretation of the high-resolution image slices. There exists a lot of variation among mouse brain datasets due to

their age, gender, choice of imaging modality and various sample preparation and staining techniques. Hence, spatial gene expression data from image slices must be registered to a common coordinate system to enable accurate inter-subject comparisons and queries of anatomical regions and sub-regions. Automating this entire process is essential for handling massive amounts of data. The Allen Brain Institute has taken on an global initiative in providing this common coordinate reference system called the Allen Reference Atlas (ARA) [16]. This atlas contains both Nissl stained slice images as well as expert-drawn annotated contour slice images from the average of slices at the same position from multiple animal subjects. Most of the previous work registers microscopic slice images to their corresponding Nissl stained slice images using intensity based approaches (Section 2). However, microscope slice images that do not share the same intensity-profile as the Nissl images have to create an intermediate atlas for registration.

In this paper, we present a novel feature based non-linear registration algorithm for automatic and robust alignment of high-resolution mouse brain slice images even with histological artifacts (tissue loss, tears and deformation) to hand-drawn annotated atlas contours. As we do not use the Nissl-based (intensity) reference space, we can register generic and typical cases of microscopic images that do not have an intensity profile similar to the atlas without using any intermediate atlas. This is significant as our approach gives the freedom to register slices from many sample preparations, using a variety of imaging modality and of any scale with the ARA maps and bring them to a common anatomical reference framework. We tested our algorithm on two complete datasets (200 slices in total), one containing highly damaged slices and the other a clean dataset from serial two-photon tomography (STPT) and show superior performance in all the tested datasets when compared with other registration algorithms.

Contributions: We present the first complete automatic registration pipeline for alignment of high-resolution mouse brain slice images with histological artifacts to a standardized atlas framework. This is critical to include the data set generated by all the conventional neuroscience research laboratories around the world. As part of the process, we propose a novel edge detection algorithm (a variant of Canny edge detector), which accurately detects all strong edges in the noisy microscopic slice images. Second, we propose an algorithm to not only identify but accurately locate and handle slice-specific histological artifacts such as tissue tears and tissue loss (missing regions) in brain slice contour edge images through Constrained Delaunay Triangulation method. Third, we solve the Laplace's equation with Dirichlet boundary conditions to perform an accurate non-linear warping of the brain slice images. Finally, we show the robustness of our algorithm through accurate alignment of over 200 mouse brain slices with and without artifacts from various parts of the brain, and on data sets acquired through two different imaging techniques.

2. RELATED WORK

In this section we discuss previous works from different areas that are most related to our proposed approach.

Detection of Artifacts. Most methods which try to automatically detect slices with artifacts look for unexpected differences between a specified slice and its neighbouring slices [13, 27]. In other words, artifacts in an isolated slice cannot be detected and corrected. Further, such a method also requires slices to be close enough and the adjacent slice to be devoid of any artifacts, such that the difference between slices will imply the artifact. There have also been efforts to not only identify but correct these artifacts. Kindle et al. [13] proposed a semi-automatic method where they manually identify small tissue tears and fill them by warping neighboring regions around the tear. This approach only works well when the tear is small, horizontal and smooth. Further, one needs to be careful about obtaining undesirable warping effects while fixing these tears, especially when they are severe as shown in Figure 4.

While the above techniques aim to detect and correct slices which have artifacts, many researchers try to overcome them. They use methods such as cryosectioning of frozen mouse brain tissue [5, 16, 3], where they embed the brain in gel like compounds making it much easier to slice tissues into thin sections without tearing or significant deformation. Another method quite popular is the introduction of quality control checks [16, 34, 20], where highly damaged slices are manually removed from the registration pipeline. A major problem with this approach is that if enough of such slices are removed, there may be not sufficient information left to register and reconstruct a 3D brain model. Further, to aid in registration of such highly damaged slices, manual landmarks are often placed [5] or even manual initial registration is performed [33, 30]. All the above measures which mitigate the 2D slice-specific artifacts and help its registration, in addition to being time consuming and expensive, require a lot of planning of the process.

Registration. There is a huge body of work on registration of medical images and the readers are referred to [19] for a detailed categorization. However, to place our work, we will briefly discuss a single classification. Registration can broadly be classified as *intra-stack*-registration among slices within a stack or *inter-stack*-registration among slices in between two stacks. Further, within each of them there exists both feature based and intensity based registration techniques.

There has been plenty of work done on *intra-stack* registration and 3D reconstruction of mouse brain by aligning serial sections, specially of autoradiography slices, using both features [9, 35, 10, 29] and intensity [22, 35]. All these works typically assume little distortion between consecutive slices and hence either use a rigid, affine, or similarity transform to get a global smooth 3D alignment. There have also been work done on *inter-stack* registration between atlas and microscope image stacks using feature based techniques. Ali et al. [1] proposed to only align the outermost contour (obtained by manual thresholding) using inflection points and area invariant descriptors by assuming a global affine transformation. Ju et al. [12] proposed a deformable subdivisional mesh based atlas to register In-Situ Hybridization (ISH) data to ARA maps using a chamber for pre-alignment of the brain tissue. On the other hand, intensity based atlas registration techniques usually rely on Nissl images and often create an intermediate atlas (either an average image [15], blockface photographs [6], manual synthetic intermediate atlas [33] or MRI images [18]) to aid in registration. Ng et al. [21] first proposed a technique for ISH to Nissl registration without using any intermediate atlas but using a region based deformable registration through warping of

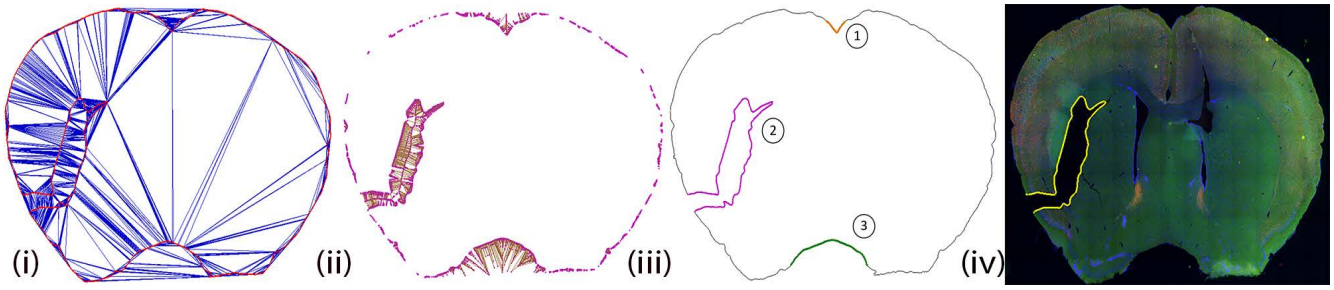

Figure 1: A. *Overview of the damaged region detection algorithm on slice* 46 *in Fig. 5:* (i). Constrained Delaunay Triangulation using the edges E and vertices V of the outermost contour of MEI. (ii). Exterior Voronoi vertices (magenta) and edges (brown) (iii). Three candidate damage areas whose Voronoi edge sequence length was above α. Points corresponding to only the 2nd candidate area was classified as damage region points as they were not vertically symmetric. (iv) Points in the damage regions (yellow) overlayed on the microscopic image (please zoom in for details)

both Nissl reference and annotated atlas image using high resolution B-spline grid. We in this paper do not perform any prealignment or assume any transformation between the atlas and the microscopic image slices. Hence, we perform a complete non-linear registration. Using our edge detection algorithm, we align *both* outer and inner contours (Fig. 3(ii)) for an accurate alignment. Aligning only the outer contours and propagating the deformation does not achieve exact interior alignment. Further, since we are directly using the annotated atlas images for registration, we only perform warping once to align the microscope image with ARA.

Although STPT produces artifact-free, well-aligned, high-resolution 3D datasets, that makes the registration process much easier [16, 28, 15], neural circuit mapping based on conventional processed brain sections continues to have technical challenges in standardized registration with highly deformed and damaged brain slices. We present methods to automatically handle such damaged slice images during our registration.

3. OVERVIEW

The input to our system are two image stacks - atlas contour images (AI) and microscopic images (MI). We use only the annotated contour information of AI that is publicly available from the Allen Brain Atlas project. We also assume that both image stacks are produced from the same slicing direction (generating coronal slices) with fixed (not necessary the same) slicing intervals. Almost all neuroanatomical labs follow a strict acquisition protocol especially for mouse brain imaging, which mostly ensures the section correspondence between AI & MI. So, given the correspondence for the first and last slices in both stacks and interval of slicing, the slice numbers of potentially matching slices of AI and MI are calculated. Given these matching slices, the rest of the paper explains the procedure to register one MI to one annotated AI.

We perform registration in four steps: (1) Robust coarse alignment of convex hulls (2) Detecting Damaged Regions (3) Global affine alignment using ICP (4) Local non-linear alignment using Laplacian.

3.1 Robust Coarse Alignment of Convex Hulls

The first step in our registration pipeline resolves the rotation component as accurately as possible. Popular methods such as principal component analysis (PCA) [11] and symmetry techniques [7] will fail when used on highly damaged MI slices (Fig. 4 and Fig. 5) because the spurious edge points produced in damaged areas of the tissues images bias the PCA; and introduce asymmetry in the structures in brain slices.

Algorithm 1 Edge threshold (K) computation for image I

1: Compute the histogram of the gradient magnitude.
2: The number of bins b in the histogram is computed using Scott's rule [31], $b = 3.49\sigma_f N^{-\frac{1}{3}}$ where σ_f=standard deviation of the N gradient magnitude values.
3: Compute first k bins such that the difference of number of points in adjacent bins lie within a fixed threshold s.
4: **return** K= Mean of gradient magnitude value corresponding to k bins.

We first create an *atlas-edge image* (AEI) by extracting the edges from AI. In order to compute the *microscopic-edge image* (MEI) from MI, whose edges corresponds to edges in AEI, we propose a novel *dominant edge detection* (DED) algorithm that is a variant of the Canny edge detector. The DED algorithm automatically computes the threshold for hysteresis to suppress the edges with low gradient magnitude as described in Algorithm 1. The automatic threshold computation uses the idea of *persistence of edges* from the histogram of the gradient magnitude. Our threshold computation algorithm performs better than the standard Otsu's method [24] as it removes small weak edges (Fig. 2), which potentially could lead to wrong correspondences.

Algorithm 1 computes threshold K from MI. After removing noise and computing the histogram, we find the first k bins, where the number of points remain stable within a fixed threshold s. Intuitively, for strong edges, the number of points in the nearby bins will not fluctuate much as compared to weak edges providing a large stable range. To compute the threshold (K) we then take the mean of the gradient magnitude values of these k bins. Lowering these values introduces weak or spurious edges. Hence, these parameters serve as a knob to control how much fitting of MI to AI is required. In our implementation we empirically found best results for $s = 12$, for which $k = 5$.

We then compute convex hulls of edge pixels in both AEI and MEI and resample it such that we have a fixed number of points uniformly sampled along the convex hull. The oriented bounding boxes (OBB) [8] of the resampled convex

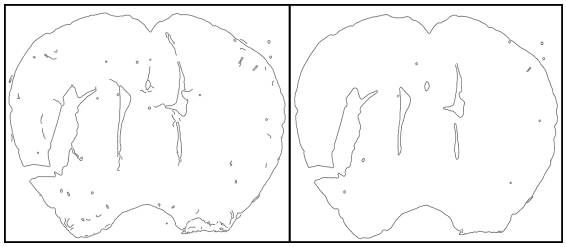

Figure 2: *Edge detection on slice* 46 *in Fig. 5:* More dominant edges are detected by our method (right) as compared to Ostu's method (left). (please zoom in for details)

hull curves of both AEI and MEI are computed using PCA. The combination of PCA on the resampled convex hull curve eliminates the edge effects including bias due to noise, tissue damage and other artifacts caused during sample preparation to which the usual edge-based registration algorithms are susceptible. From the OBB, relative coarse translation, scaling, and rotation are robustly computed between AEI and MEI.

3.2 Detecting Damaged Regions

Before computing corresponding points between MEI and AEI, and using those to further align the two images, it is important to first accurately identify and remove points in the damage regions. The presence of edges due to the damage regions misleads and corrupts the correspondence finding (Fig. 3(i)), resulting in bad registration.

Our algorithm to detect damage regions in mouse brain slice images is motivated by two key observations. First, the contours of most of the damaged regions have long exterior medial axis creating deep concavity into the tissue. It is quite rare that the tear happens in the interior of the tissue directly without affecting the boundary of the tissue. Second, the damage region exhibits vertical asymmetry between left and right regions of the mouse brain. It is also very rare that the same type and shape of tear or missing region happens on both lobes of the brain tissue slice.

Algorithm 2 computes points P_D in the damaged regions in MEI. First, we construct a Constrained Delaunay triangulation (CDT) using vertices V and edges E from the outermost contour of MEI (Fig. 1(i)). We then remove the Voronoi vertices and edges corresponding to the internal triangles in its dual Voronoi diagram (Fig. 1(ii)). After which we identify the Voronoi edge sequences (medial axis) [2] that are long (above the given threshold α; we use $\alpha = 20$) – their corresponding vertices in V are the points in the candidate damaged regions (Fig. 1(iii)). There may be important features of the brain that may also have long medial axis, but these features are also symmetric on both sides of the brain. Therefore we finally check if the candidate regions are vertically symmetric: the points in the candidate damaged regions are reflected along the vertical axis of the OBB (computed in Section 3.1) and for every reflected point, a small 3x3 neighbourhood region is checked for vertices in the original data set with similar normal vectors. If no such points are found, then it is declared that there is no symmetry, the points in the identified region are classified as damaged area points and removed from MEI (Fig. 3(ii)).

Algorithm 2 Detection of points P_D in the damaged regions in input MEI.
INPUT: Vertices V & Edges E from outermost contour of MEI and α.
OUTPUT: Points P_D in the damaged regions of MEI

1: Construct a CDT [4] using E & V.
2: Remove all the triangles inside the polygon formed by E. Also remove all the sliver triangles whose circumcenter does not lie inside their triangle.
3: Using the remaining E & V, construct the dual Voronoi diagram.
4: Compute all the Voronoi edge sequences $\geq \alpha$ and let the triangle vertices V corresponding to the remaining Voronoi vertices be V'.
5: Check for vertical symmetry $\forall\ v \in V'$ and remove symmetric vertices from V'.
6: **return** $P_D \Leftarrow V'$ which are asymmetric.

3.3 Global Affine Alignment using ICP

As both MEI and AEI are coarsely aligned (from Section 3.1), we assume that rotation component is resolved and only the translation and scaling components needs correction. Hence, for corresponding points on the edge curves of AEI and MEI, we can assume that the normal vectors would be almost the same. We compute the normal vectors of the points in AEI and the remaining points (after removing the damaged regions) in MEI using moving least squares [17] as it smoothly interpolates the normal vectors, diminishing the effect of noise, sharp features and topological foldings. Using these normal vectors as features, we then search for corresponding points between AEI and MEI within a small angle threshold. We may find multiple points in the AEI in a small neighborhood corresponding to a single point in MEI. We assign weighted average of these multiple matches in AEI based on its Euclidean distance from the point in MEI, as the target position to which that MEI point should be finally moved. To exclude incorrect matches, we check if points in the neighborhood of a point in MEI are matched to the points in the same neighborhood in AEI. Using these robust correspondences, the affine transformation matrix is computed using linear least

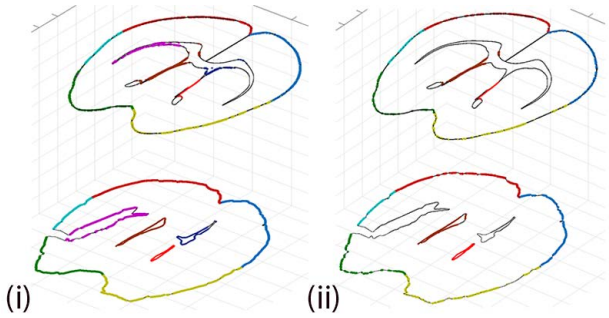

Figure 3: *Correspondences after initial coarse alignment of slice* 46 *in Fig. 5 and its atlas:* Dense correspondences before (left) and after (right) outlier removal (damage region + incorrect correspondences) between MEI (bottom) and its corresponding atlas (top). Correspondences are shown using similarly colored curve segments. (please zoom in for details)

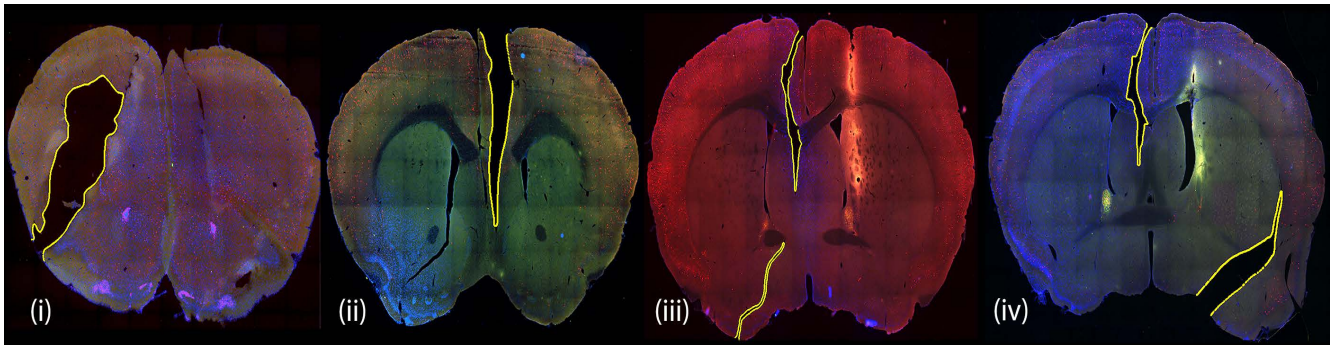

Figure 4: *Results of our automatic damage region detection algorithm:* The figure shows the results of our algorithm on a sample of four high-resolution mouse brain slice images with single or mutiple histological artifacts (tears and missing data). We successfully identified the contours of the damage regions (yellow) in all four images (background). (please zoom in for details)

square formulation that would take the points in MEI as close as possible to their corresponding matching points in AEI. The global transformation thus computed may have non-uniform scaling, shear, and possibly a minor rotation adjustment component too. So, this transformation would change the normal vector of the points in MEI, which would lead a slightly different set of matching points from AEI in the subsequent iteration, and potentially a different transformation matrix that would take MEI points further close to their new matches. Since we also use the distance of AEI points from the MEI (in the aligned images) for pruning the matching set of points, this *iterative closest point* optimization will converge. We used progressively tighter normal vector angle deviation thresholds $(10°, 8°, 6°, 4°)$ and smaller distance threshold $\left(\frac{1}{10}, \frac{1}{20}, \frac{1}{40}, \frac{1}{80}\right)$ of image-height in each iteration for quicker convergence.

3.4 Local Non-Linear Alignment using Laplacian

After global affine transformation, we compute the final list of corresponding points between MEI and AEI that are spatially $\left(\frac{1}{40}\right)$ of image-height pixels apart, and deviate no more than 1 degree in their normal vectors. Given such tight correspondences, the next step is to register these points with each other using non-linear alignment technique. Let points in MEI, P_M, whose corresponding points in AEI, P_A, be given. This image warping function, $\phi(x, y)$, posed as the solution to Laplace's equation [25], should take each point in P_M to its corresponding point in P_A. For points in P_M, this function is given as Dirichlet boundary condition $\phi(s,t) = (B_x(s,t), B_y(s,t)), (s,t) \in P_M$, where B is the displacement vector between the corresponding points. Other pixels are distorted as little as possible by this warping function: $\phi(s,t) = 0, \forall (s,t) \notin P_M$. The smoothness in warping is achieved by the following Laplace's equations:

$$\nabla\phi_x = \frac{d^2\phi_x}{dx^2} + \frac{d^2\phi_x}{dy^2} = 0 \quad \nabla\phi_y = \frac{d^2\phi_y}{dx^2} + \frac{d^2\phi_y}{dy^2} = 0 \quad (1)$$

By approximating the second derivative at nodal point (x, y) (derived from Taylor series), the finite difference approximation of Laplace's equation for interior regions can be expressed as a homogeneous system of linear equations of form

$$\phi(x,y) = \frac{1}{4}\big(\phi(x+1,y) + \phi(x-1,y) + \phi(x,y+1) + \phi(x,y-1)\big) = 0 \quad (2)$$

Combining the above equations and representing it in matrix notation gives, $A\phi_x = C_x$ and $A\phi_y = C_y$, where A is a matrix $m \times m$ and m is the number of pixels in MI. The row vectors of A takes the coefficients of terms in Equation 2 except for the rows corresponding to MEI points in which case, it represents the Dirichlet boundary condition. The vector C_x and C_y are zero everywhere except for the rows corresponding to MEI points in which case it is B_x and B_y respectively. Note that A is a sparse matrix allowing for efficient computation of the solution of ϕ that minimizes the residual, $\| C - A\phi \|$.

4. RESULTS & DISCUSSION

We evaluate our method on 200 images of coronal mouse brain slices (5000 x 8000 pixels) with a resolution of $0.6\mu m$ per pixel. To test the robustness of our method, these images were taken from different datasets spanning different regions of the brain. Of these, 60 slices were from STPT[1] (with no major artifacts) and the rest 140 produced from conventional processing techniques [32, 23]. Our registration results for all 200 slices (Fig. 5 & 6) were found qualitatively quite accurate by the subject experts. The complete algorithm to align a damaged histological slice with its corresponding ARA maps takes 1 minute with our unoptimized MATLAB code on an Intel Core i5 CPU with 8GB RAM. We also perform quantitative evaluation and comparison of our method with a similar end-to-end intensity based registration method that uses mutual information as its similarity metric. We chose mutual information because it is the most commonly used and popular metric for such *inter-stack* registration problems (ISH to ARA) [26, 21]. We implemented the above method in Elastix [14], an ITK based modular framework, where we optimized all the parameters for the best overall performance. We used Advanced Mattes mutual information to register the DAPI stained MI with the Nissl image from ARA maps by performing an *affine registration* followed by an *elastic cubic B-spline* based transformation

[1]Publically available from the Allen Brain Atlas Project

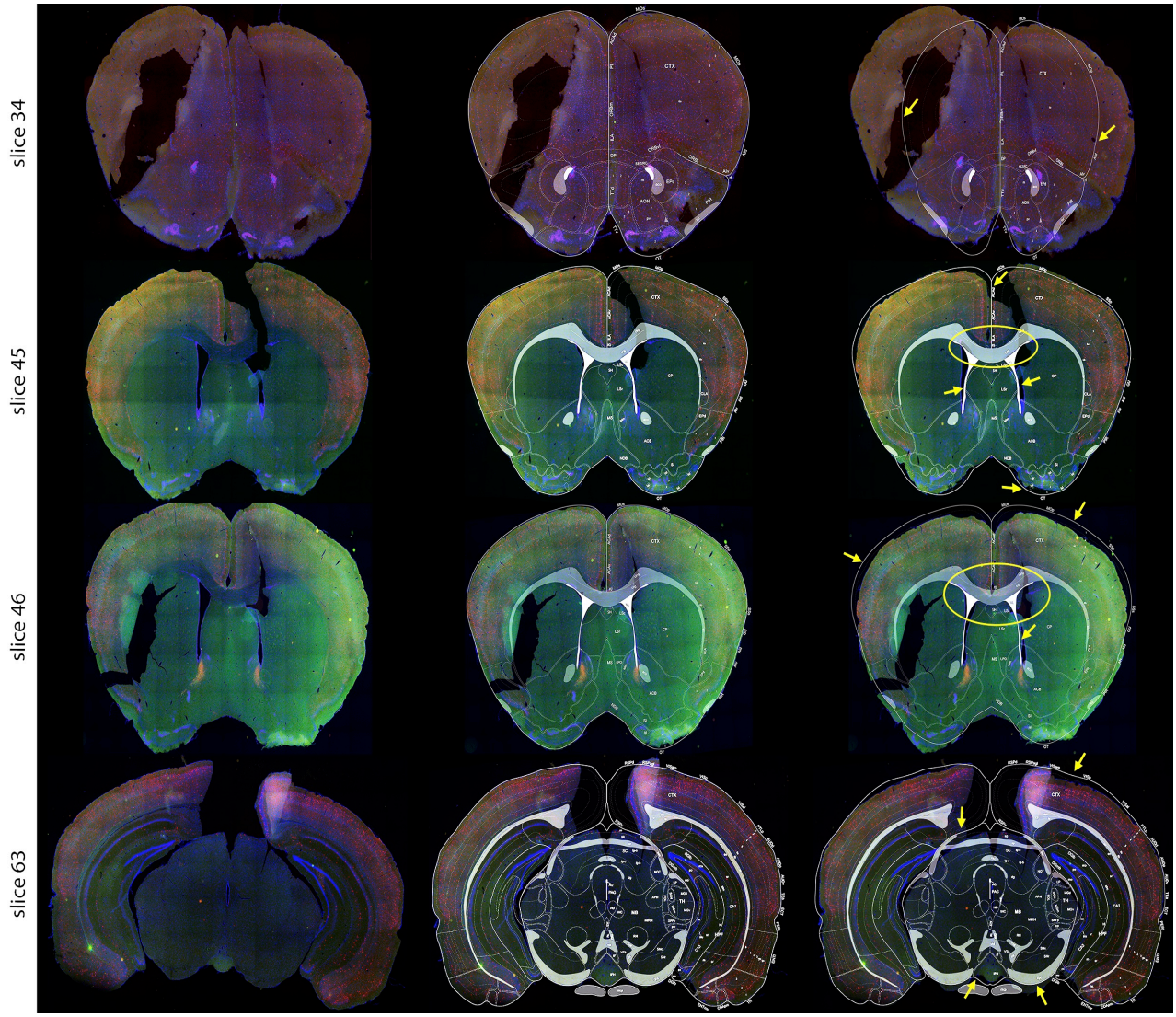

Figure 5: *Comparison of registration results on damaged slices:* First column shows damaged coronal slices from conventional histological processing techniques. Second column shows results from our registration algorithm on the these slices with the corresponding atlas overlayed in white. Third column shows results from affine + non-linear B-spline registration using Elastix with the corresponding atlas overlayed in white. A few sample locations of incorrect registration in the third column is shown using yellow arrows and marked regions. (please zoom in for details)

using a multi-resolution approach. An adaptive stochastic gradient descent optimizer with the final B-spline grid spacing of $11\mu m$ was used to ensure matching of local structures.

We compared the root-mean-squared error (RMSE), the median error (MEE) and the maximal error (MAE) of 20 corresponding points which were manually picked and distributed uniformly in MI and AI pair. This comparison was done only for 140 slices from conventional processing techniques as there were no corresponding Nissl images for slices from STPT. Although damage identification is done automatically, in order to collect statistics on results and for comparison with other methods, damaged slices were manually identified by subject experts, separated from clean slices, and separate comparisons were done on those slices.

There are two stages (affine & non-linear) to the pipeline and the two registration methods have different algorithms to realize each of these stages. The results in Table 1 are reported after each of the two stages. We found that during affine registration of damaged slices (52 slices), our proposed method gives lower registration errors (in terms of average RMSE & MAE) as compared to the intensity based method. For clean slices (88 slices) both performed equally well. After the non-linear registration, even in clean slices, we performed slightly better than intensity based method in all statistical measurements as we are using Laplace's equations. Laplace equations, like thin plate spline (TPS) or B-spline also minimizes the total curvature. The addition of point correspondences as Dirichlet boundary conditions further constrains the interpolation of the displacement functions for an accurate MI to AI alignment.

Discussion. Histological analysis is still the gold-standard for the accurate description of neuroanatomy and for tissue

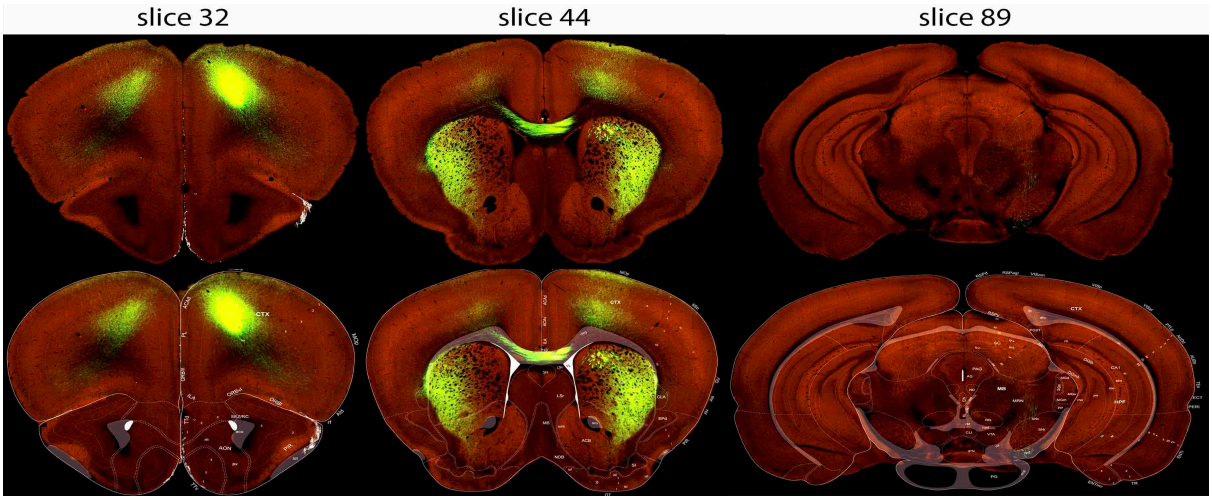

Figure 6: *Registration results of our algorithm on clean slices:* The first row shows coronal slices from STPT while second row shows registration results with the corresponding atlas overlayed in white. (please zoom in for details)

characterization of the mouse brain. Since our goal is to create a database by bringing all these histology slice images (clean or damaged) to a common anatomical framework (like ARA maps) and also gather statistics about common expression patterns in anatomical structures across experiments, it is vital that we achieve an accurate and robust registration. We do this by aligning only the outer and inner contours of the microscopic and the annotated atlas images. Note as we do not use the Nissl-based (intensity) atlas images from ARA, our method can align even those microscopic images that do not share a similar intensity-profile as the atlas. Another advantage of our method is that it can handle slice-specific histological artifacts such as tissue tears and tissue loss, which are very common in conventionally processed slices. Both these benefits allow our algorithm to align more brain datasets to ARA maps for a more thorough and extensive connectome studies.

Our robust damage detection algorithm can accurately detect multiple artifacts that may be present in a single slice images (Fig. 4(iii) and Fig. 4(iv)). This enables and facilitates extremely thin sectioning of the mouse brain tissue, which is necessary for an accurate 3D mouse brain model reconstruction. However, there are still some extreme deformations that would be difficult to handle with our algorithm. For deformations such as folding of the tissue and overlap of adjacent tissue regions, a more complicated or semi-automatic approach might be helpful. Another extreme deformation present usually in the bottom slices (posterior) is the relative displacement of left and right lobes of the mouse brain tissue. For such slices, a combination of our method and a sub-region (block) registration [6] might be more helpful .

Although at present, we manually select the ids of the top and bottom matching images in both stacks, we would like to automate this also for an accurate registration of the complete 3D dataset, using a good error metric for alignment. Currently this is extremely challenging due to two factors. Firstly, since we do not freeze the tissue, there is an uneven distribution of mass in the interior of the tissue due to gravity. Secondly, since we do not use any chamber for pre-alignment of the brain tissue like [12, 16], we need to account for the slicing direction. In future we would like to address both these issue for an accurate 3D reconstruction of serial slices.

5. SUMMARY

To the best of our knowledge the presented work is the first to automatically register highly damaged, high-resolution optical slice images of mouse brain to hand-drawn atlas contours without using any intermediate atlas. We align only the contours of the microscopic and annotated ARA atlas images. This is significant as contours can always be extracted from intensity images, making our algorithm always applicable. However, intensity based approaches cannot be applied if the two images have different intensity profiles. Our robust damaged region detection with contour registration technique condones histological artifacts that occur in standard procedures to produce brain slices. We envision our technique to complement existing registration algorithms so that more data can be aligned with ARA maps.

6. REFERENCES

[1] W. S. I. Ali et al. Registering coronal histological 2-d sections of a rat brain with coronal sections of a 3-d brain atlas using geometric curve invariants and b-spline representation. *Medical Imaging, IEEE Transactions on*, 17(6):957–966, 1998.

[2] N. Amenta, M. Bern, and D. Eppstein. The crust and the β-skeleton: Combinatorial curve reconstruction. *Graphical models and image processing*, 60(2):125–135, 1998.

[3] L. Bertrand and J. Nissanov. The neuroterrain 3d mouse brain atlas. *Frontiers in neuroinformatics*, 2:3, 2008.

[4] L. P. Chew. Constrained delaunay triangulations. *Algorithmica*, 4(1-4):97–108, 1989.

[5] A. C. Crecelius, D. S. Cornett, R. M. Caprioli, et al. Three-dimensional visualization of protein expression in mouse brain structures using imaging mass spectrometry. *J. Am. Soc. Mass Spectrom.*, 16(7):1093–1099, 2005.

Table 1: Comparison of registration errors (in pixels) after affine & final non-linear (affine+elastic) transformations using intensity-based & our feature-based method.

		Clean Slices (88 slices)			**Damaged Slices** (52 slices)		
		Average RMSE	Average MEE	Average MAE	Average RMSE	Average MEE	Average MAE
After Affine Transformation	Intensity-Based	11.79	9.33	24.71	18.96	11.55	40.57
	Proposed	12.91	10.58	23.92	13.37	10.66	25.27
After Non-Linear Transformation	Intensity-Based	4.68	3.20	8.03	8.88	6.55	24.69
	Proposed	3.61	2.51	5.7	3.91	2.53	6.01

[6] J. Dauguet, T. Delzescaux, F. Condé, et al. Three-dimensional reconstruction of stained histological slices and 3d non-linear registration with in-vivo mri for whole baboon brain. *J. Neurosci. Meth.*, 164(1):191–204, 2007.

[7] N. Gelfand et al. Robust global registration. In *SGP*, volume 2, pages 197âĂŤ–206, 2005.

[8] S. Gottschalk, M. C. Lin, and D. Manocha. Obbtree: A hierarchical structure for rapid interference detection. In *Proceedings of Annual conference on Computer graphics and interactive techniques*, pages 171–180. ACM, 1996.

[9] A. Hess et al. A new method for reliable and efficient reconstruction of 3d images from autoradiographs of brain sections. *J. Neurosci. Meth.*, 84(1):77–86, 1998.

[10] L. S. Hibbard and R. A. Hawkins. Objective image alignment for three-dimensional reconstruction of digital autoradiograms. *J. Neurosci. Meth.*, 26(1):55–74, 1988.

[11] I. Jolliffe. *Principal component analysis*. Wiley Online Library, 2002.

[12] T. Ju, J. Warren, G. Eichele, C. Thaller, et al. A geometric database for gene expression data. In *Symp. on Geometry Processing (SGP)*, pages 166–176, 2003.

[13] L. M. Kindle, I. A. Kakadiaris, T. Ju, and J. P. Carson. A semiautomated approach for artefact removal in serial tissue cryosections. *J. Microsc.*, 241(2):200–206, 2011.

[14] S. Klein, M. Staring, et al. Elastix: a toolbox for intensity-based medical image registration. *Medical Imaging, IEEE Transactions on*, 29(1):196–205, 2010.

[15] L. Kuan, Y. Li, C. Lau, D. Feng, A. Bernard, et al. Neuroinformatics of the allen mouse brain connectivity atlas. *Methods*, 73:4–17, 2015.

[16] E. S. Lein, M. J. Hawrylycz, N. Ao, et al. Genome-wide atlas of gene expression in the adult mouse brain. *Nature*, 445(7124):168–176, 2007.

[17] D. Levin. The approximation power of moving least-squares. *Math. of Computation*, 67(224):1517–1531, 1998.

[18] Y. Ma et al. Three-dimensional digital atlas database of adult c57bl/6j mouse brain by magnetic resonance microscopy. *Neuroscience*, 135(4):1203–1215, 2005.

[19] J. B. Maintz et al. A survey of medical image registration. *Med Image Anal*, 2(1):1–36, Mar 1998.

[20] K. Mosaliganti, T. Pan, R. Sharp, et al. Registration and 3d visualization of large microscopy images. In *SPIE Medical imaging*, pages 61442V–61442V. International Society for Optics and Photonics, 2006.

[21] L. Ng et al. Automated high-throughput registration for localizing 3d mouse brain gene expression using itk. In *Insight J. MICCAI Workshop*, 2005.

[22] C. Nikou et al. Robust statistics-based global energy function for alignment of serially acquired autoradiographic sections. *J. Neurosci. Meth.*, 124(1):93–102, 2003.

[23] S. W. Oh, J. A. Harris, L. Ng, B. Winslow, N. Cain, et al. A mesoscale connectome of the mouse brain. *Nature*, 508(7495):207–214, 2014.

[24] N. Otsu. A threshold selection method from gray-level histograms. *Automatica*, 11(285-296):23–27, 1975.

[25] P. Pérez, M. Gangnet, and A. Blake. Poisson image editing. In *ACM Transactions on Graphics (TOG)*, volume 22, pages 313–318. ACM, 2003.

[26] J. P. Pluim, J. A. Maintz, et al. Mutual-information-based registration of medical images: a survey. *Medical Imaging, IEEE Transactions on*, 22(8):986–1004, 2003.

[27] X. Qiu, T. Pridmore, and A. Pitiot. Correcting distorted histology slices for 3d reconstruction. *Med Image Underst Anal*, 2009.

[28] T. Ragan, L. R. Kadiri, et al. Serial two-photon tomography for automated ex vivo mouse brain imaging. *Nature methods*, 9(3):255–258, 2012.

[29] A. Rangarajan, H. Chui, et al. A robust point matching algorithm for autoradiograph alignment. *Medical Image Analysis*, 1(4):379–398, 1997.

[30] S. J. Sawiak, G. B. Williams, N. I. Wood, et al. Spmmouse: A new toolbox for spm in the animal brain. In *ISMRM 17th Scientific Meeting & Exhibition, April*, pages 18–24, 2009.

[31] D. W. Scott. On optimal and data-based histograms. *Biometrika*, 66(3):605–610, 1979.

[32] Y. Sun et al. Cell-type-specific circuit connectivity of hippocampal ca1 revealed through cre-dependent rabies tracing. *Cell reports*, 7(1):269–280, 2014.

[33] D. A. Vousden, J. Epp, H. Okuno, et al. Whole-brain mapping of behaviourally induced neural activation in mice. *Brain Structure and Function*, pages 1–15, 2014.

[34] P. A. Yushkevich, B. B. Avants, L. Ng, et al. 3d mouse brain reconstruction from histology using a coarse-to-fine approach. In *Biomedical Image Registration*, pages 230–237. Springer, 2006.

[35] W. Zhao, T. Y. Young, and M. D. Ginsberg. Registration and three-dimensional reconstruction of autoradiographic images by the disparity analysis method. *Medical Imaging, IEEE Transactions on*, 12(4):782–791, 1993.